Arabian Journal of Chemistry (2019) **12**, 4035–4043

King Saud University

Arabian Journal of Chemistry

www.ksu.edu.sa
www.sciencedirect.com

ORIGINAL ARTICLE

Synthesis of $SmLuO_3$ and $EuLuO_3$ interlanthanides from hydrothermally-derived nanostructured precursors

Júlia C. Soares [a], Kisla P.F. Siqueira [a], Roberto L. Moreira [b], Anderson Dias [a,*]

[a] *Departamento de Química, Universidade Federal de Ouro Preto, Campus Morro do Cruzeiro, ICEB II, Ouro Preto, MG 35400-000, Brazil*
[b] *Departamento de Física, ICEx, Universidade Federal de Minas Gerais, C.P. 702, Belo Horizonte, MG 30123-970, Brazil*

Received 5 January 2016; accepted 31 March 2016
Available online 20 April 2016

KEYWORDS

Interlanthanides;
Rare earth;
Hydrothermal;
Raman spectroscopy;
Sesquioxides

Abstract Phase-pure cubic $SmLuO_3$ and $EuLuO_3$ interlanthanides were synthesized for the first time from nanostructured hydrothermally-derived precursors. LuO(OH), $Sm(OH)_3$ and $Eu(OH)_3$ materials were firstly obtained by hydrothermal synthesis at 250 °C for 24 h. X-ray diffraction, micro-Raman spectroscopy, scanning and transmission electron microscopies were employed to investigate the thermal behavior of the mixed systems $Sm(OH)_3$–LuO(OH) and $Eu(OH)_3$–LuO(OH), up to 1600 °C. It was observed that the precursors were converted to lanthanide oxides in the temperature range 800–1200 °C, followed by chemical reactions that allowed the production of a mixture of monoclinic and cubic $SmLuO_3$ or $EuLuO_3$ materials at 1400 °C. Phase-pure cubic ($Ia\bar{3}$ space group, #206) interlanthanides were produced at 1600 °C, as corroborated by micro-Raman scattering probing the phonon modes, which were determined and assigned. The results showed that both systems could be promising materials for optical applications.
© 2016 The Authors. Published by Elsevier B.V. on behalf of King Saud University. This is an open access article under the CC BY-NC-ND license (http://creativecommons.org/licenses/by-nc-nd/4.0/).

1. Introduction

Interlanthanide oxides with general formula $LnLn'O_3$, also called ternary lanthanide oxides, have received special attention in the last years because of their remarkably complex structures that lead to potentially tunable optical (Blanusa et al., 2008), magnetic (Ito et al., 2001; Mele et al., 2009), and microwave-related properties (Moreira et al., 2005; Sharma et al., 2015). Many simple binary sesquioxides of trivalent lanthanides were investigated recently due to their intricate crystal chemistry, since they can be found in three different structures ranging from cubic fluorite-type (C-type), hexagonal A-type, to monoclinic B-type, with many scientific and technological applications (Mele et al., 2003; Peng and Zhang, 2007; Chung and Lee, 2004; Azimi et al., 2013; Yang et al., 2008; Hao et al., 2010). In particular,

* Corresponding author. Tel.: +55 31 35591716; fax: +55 31 35591707.
E-mail address: anderson_dias@iceb.ufop.br (A. Dias).
Peer review under responsibility of King Saud University.

Production and hosting by Elsevier

http://dx.doi.org/10.1016/j.arabjc.2016.03.010
1878-5352 © 2016 The Authors. Published by Elsevier B.V. on behalf of King Saud University.
This is an open access article under the CC BY-NC-ND license (http://creativecommons.org/licenses/by-nc-nd/4.0/).

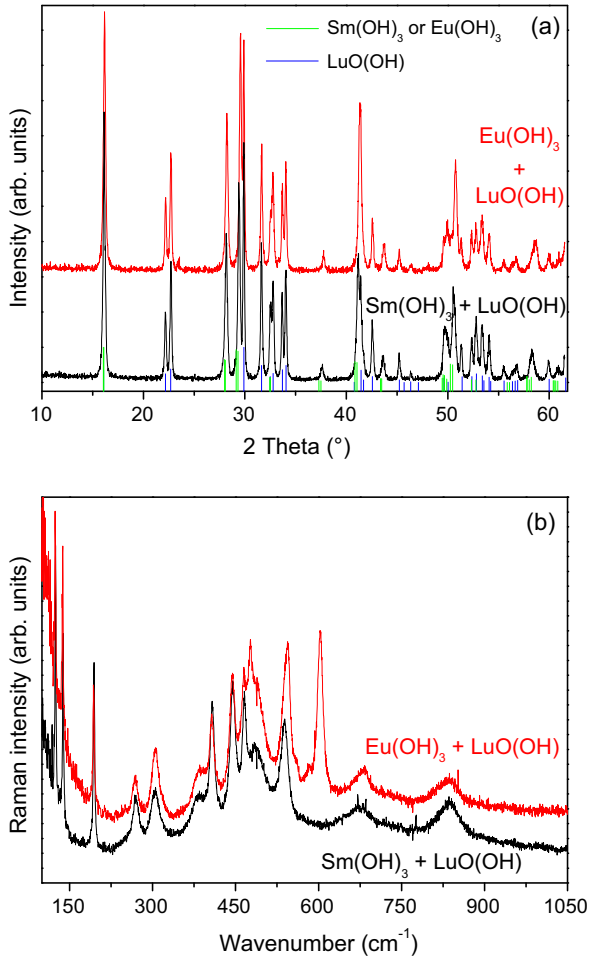

Figure 1 (a) XRD patterns and (b) Raman spectra for the hydrothermally-synthesized [$Sm(OH)_3$ + LuO(OH)] and [$Eu(OH)_3$ + LuO(OH)] precursors at 250 °C.

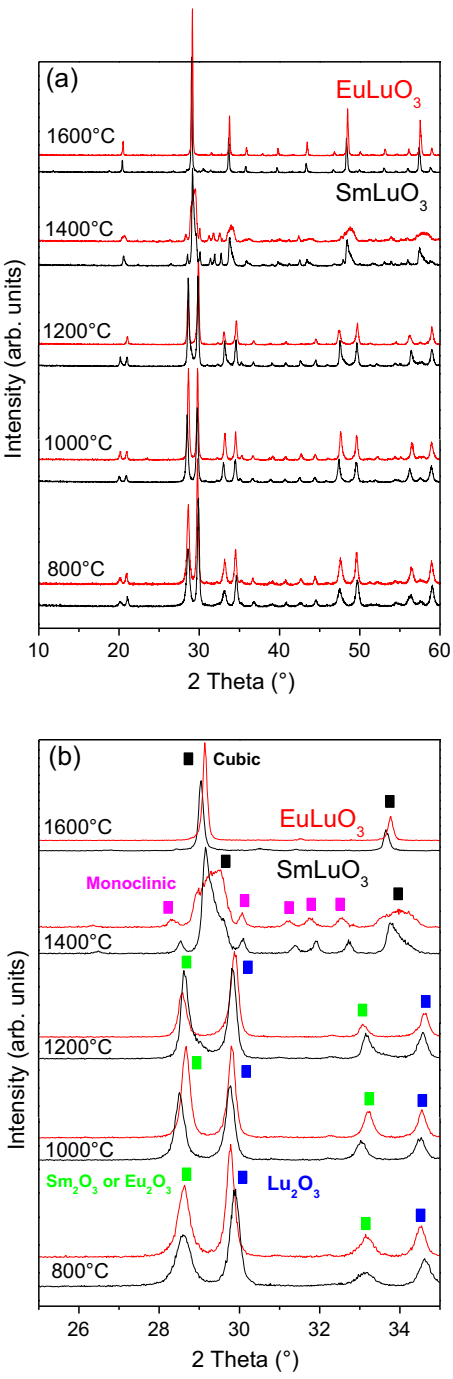

Figure 2 XRD patterns for samples produced in the temperature range 800 °C, 1000 °C, 1200 °C, 1400 °C and 1600 °C (from bottom to top). (a) General XRD patterns in the 10–60° 2Θ range, and (b) particular view with peak identification of different phases (in color) in the region 25–35° 2Θ.

samarium and europium oxides are technologically important compounds due to their optical (Martel et al., 1998; Dakhel, 2004a), magnetic (Zhang and Zhu, 2009) and catalytic properties (Gao et al., 2002). For example, it is well known that europium oxide stands out for its light emissive and electrically insulating properties (Shionoya and Yen, 1999; Dakhel, 2004b; Singh et al., 2008). In the last decades, many works have investigated a large number of trivalent lanthanide combinations in order to obtain potentially ordered ternary mixed-lanthanide phases by systematically substituting smaller ions into lower coordination sites and larger ions into higher coordination sites (Ito et al., 2001; Mele et al., 2009; Moreira et al., 2005; Sharma et al., 2015; Bharathy et al., 2009; Dubok et al., 2003). Of course, problems related to order–disorder phenomena in these ternary compounds may occur, which can be advantageous from the perspective of doping (disordered materials) or from the point of view of the polymorphism (ordered materials). All combinations, however, deserve investigations toward a deep exploration of structure–property relationships where different lanthanide ions are structurally distinct.

This work focuses on the investigation of interlanthanides $SmLuO_3$ and $EuLuO_3$. Both compositions were firstly synthesized by Schneider and Roth (1960) at high temperatures. The authors studied various binary mixtures of lanthanide oxides in different proportions by solid-state reactions. In that study, Schneider and Roth reported a mixture of cubic and monoclinic phases for $SmLuO_3$, and a phase-pure cubic for $EuLuO_3$ after heat treatments at 1650 °C for 6 h, not presenting, however, any X-ray diffraction (XRD) data. Su et al. (1988) studied eighteen years later the interlanthanide $EuLuO_3$. This material was synthesized with a combination of high pressure and temperature (3 GPa and 1200 °C), obtaining phase-pure monoclinic samples under these extreme conditions. Bharathy et al. (2009) presented a structure map for all known interlanthanides in the literature, which shows that $EuLuO_3$ is known as belonging to a monoclinic structure. Another work of Su et al. (1989) was cited by Bharathy et al. (2009) as an example of previous investigation on $EuLnO_3$ materials.

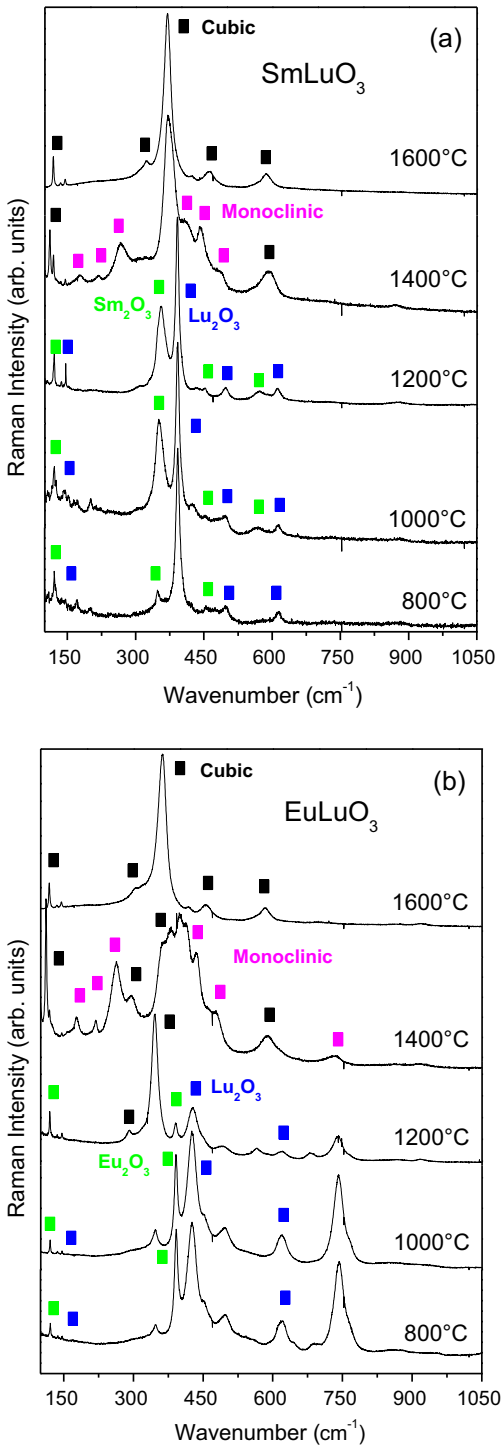

Figure 3 Raman spectra (50–1050 cm^{-1} range) for samples produced in the temperature range 800 °C, 1000 °C, 1200 °C, 1400 °C and 1600 °C (from bottom to top) from hydrothermally-processed precursors at 250 °C, aiming to the production of phase-pure cubic (a) $SmLuO_3$ and (b) $EuLuO_3$.

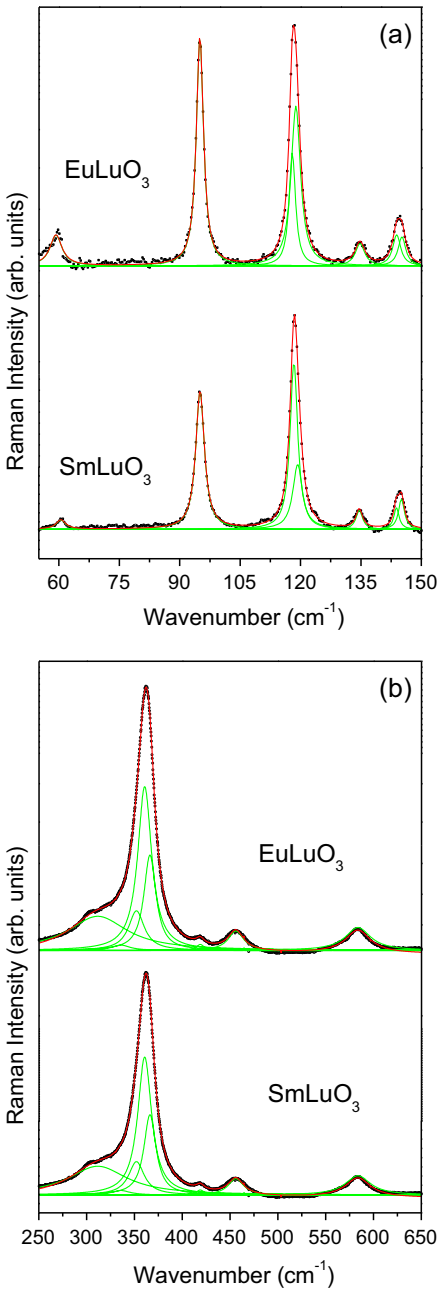

Figure 4 Micro-Raman spectra for $SmLuO_3$ and $EuLuO_3$ samples in the spectral regions (a) 50–150 cm^{-1} and (b) 250–650 cm^{-1}. Experimental data are in open circles, whereas the fitting curves are represented by red lines. Green lines represent the phonon modes adjusted by Lorentzian curves.

Nevertheless, Su et al. (1989) have indeed studied $LnEuO_3$ materials, with europium on *B*-sites in combination with large lanthanide ions, such as Sm^{3+}, Nd^{3+}, Pr^{3+}, Ce^{3+}, and La^{3+}. Tamburini et al. (2009) have recently investigated the formation of lanthanide complexes starting from macrocyclic ligands. These authors verified that the thermal decomposition of heterodinuclear europium complexes leads to the formation of $EuLuO_3$, not showing however any XRD data or information regarding the crystal phase of this final product.

Many synthetic methods were employed to produce binary and ternary lanthanide oxides as powders, single crystals or films. Although the standard solid-state reaction constitutes the main processing route for these materials (Ito et al., 2001; Moreira et al., 2005; Sharma et al., 2015), other non-conventional methods are also currently applied, such as reverse-strike coprecipitation (Tompsett et al., 1998), mechanochemical (Tsuzuki et al., 1998), thermal decomposition (Mele et al., 2003; Mele et al., 2009; Dubok et al., 2003; Artini et al., 2011; Ubaldini and

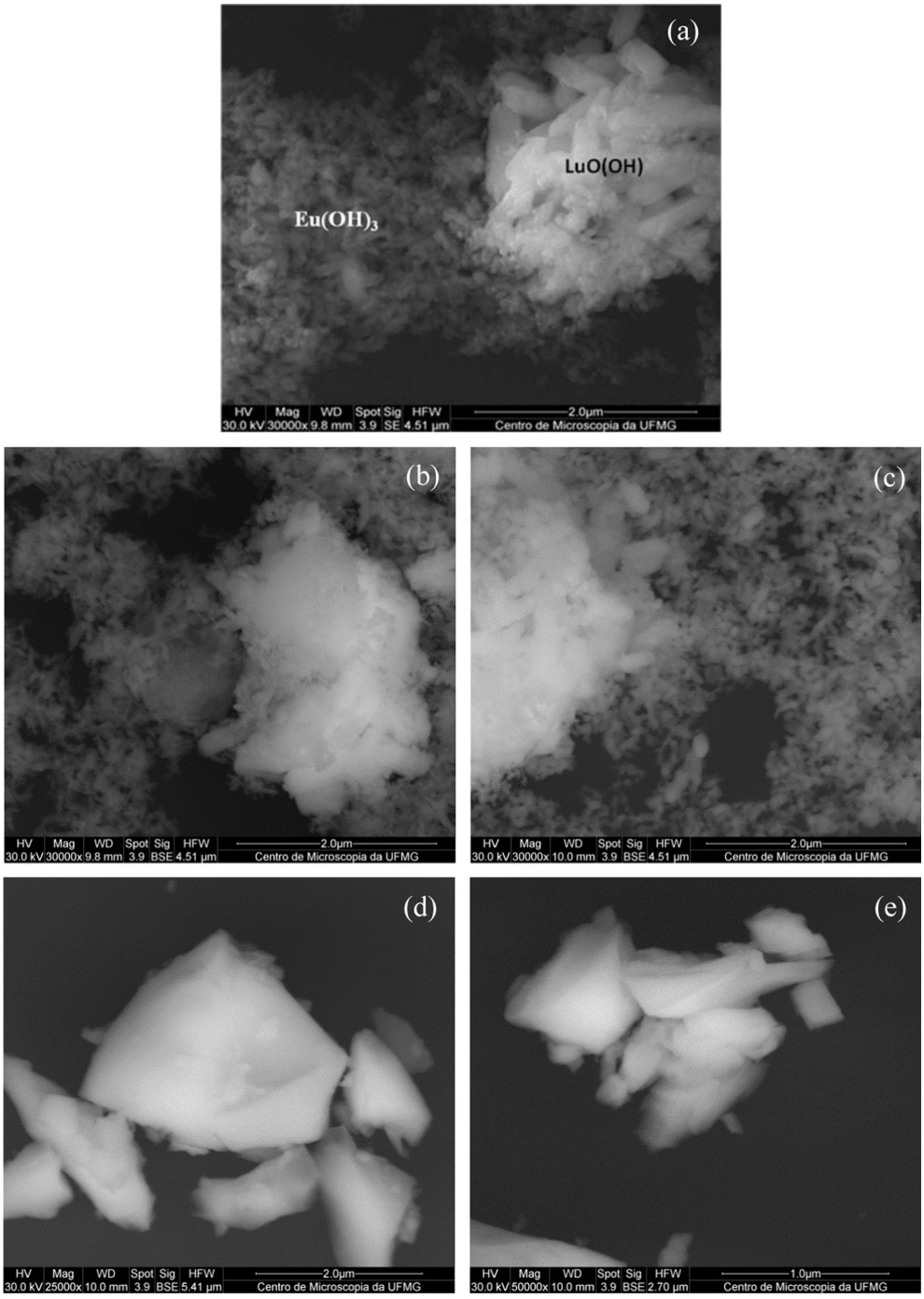

Figure 5 SE–FESEM and BSE–FESEM images for samples obtained at different conditions. (a) Precursors obtained by hydrothermal synthesis at 250 °C; samples calcined at (b) 800 °C, (c) 1000 °C, (d) 1400 °C and (e) 1600 °C.

Carnasciali, 2008; Antic et al., 2010), sol–gel processing (Heiba et al., 2003; Heiba et al., 2005; Heiba et al., 2012), combustion synthesis (Panitz et al., 2000), molecular beam epitaxy technique (Wang et al., 2010; Paranthaman et al., 1999), and hydroxide fluxes (Bharathy et al., 2009). Our research group currently works with the hydrothermal technology to synthesize nanostructured materials with practical interest (Dias and Ciminelli, 2003; Dias and Moreira, 2007; Dias et al., 2001; Dias et al., 2007; Dias et al., 2009; Siqueira et al., 2010; Siqueira and Dias, 2011). In these previous investigations, our goal was to show that phase behavior as well as morphology of the nanopowders can be tailored in selected systems by choosing the appropriate feed chemistry and processing conditions during hydrothermal syntheses. To achieve this purpose, we have used equipments and setups which allowed fully-controlled temperature–pressure–time–pH environments. Thus, potentially reactive materials could be produced in mild, reliable and reproducible conditions. As it is well known, these synthesis parameters have strong influence on the crystal structure, purity, ordering degree, particle size and morphology of the resulting compounds (Byrappa and Yoshimura, 2001; Yoshimura and Byrappa, 2008). Since all these aspects determine the properties and performance of the advanced materials, the investigation of their processing conditions becomes very important in this context.

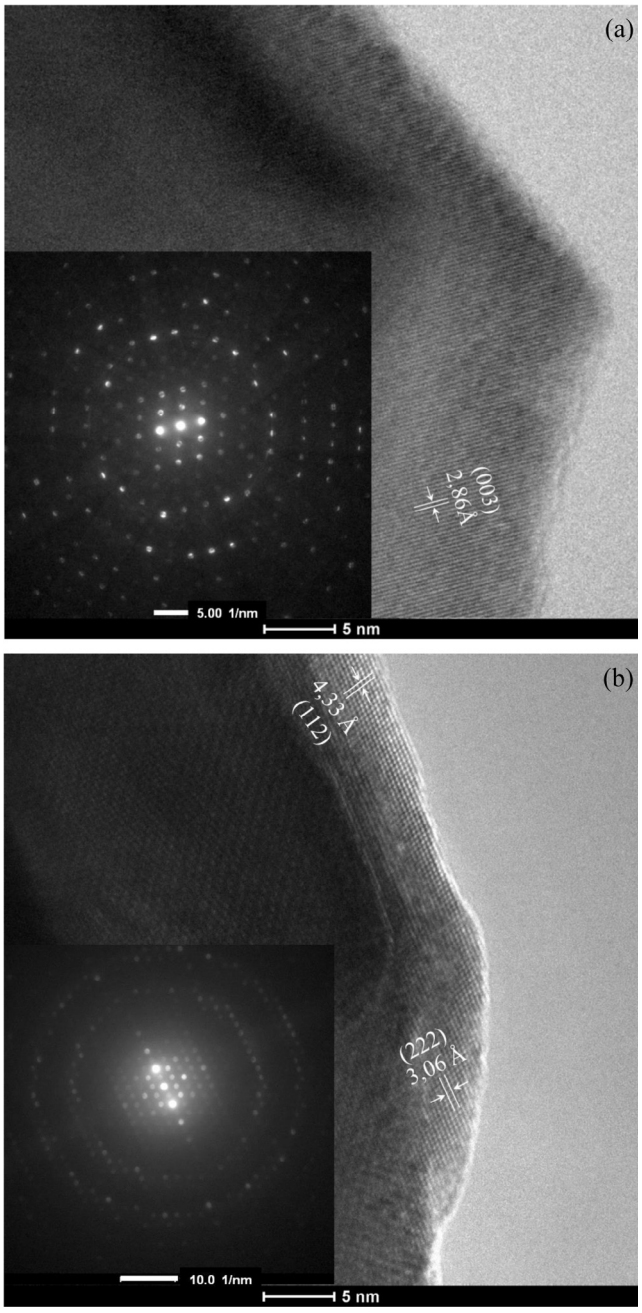

Figure 6 HRTEM images and NBD patterns for the $EuLuO_3$ materials produced at 1400 °C and 1600 °C. (a) Secondary monoclinic phase detected in samples obtained at 1400 °C, with interplanar spacing corresponding to the (0 0 3) planes of the *C2/m* space group. (b) Phase-pure $EuLuO_3$ samples obtained at 1600 °C, with interplanar spacings corresponding to the (1 1 2) and (2 2 2) planes of the cubic $Ia\bar{3}$ space group. Insets exhibit NBD patterns for the samples with different crystal structures, observed by XRD and HRTEM.

In view of the aforesaid discussion, this work introduces the hydrothermal processing route for the production of highly reactive nanostructured precursors (in particular $Sm(OH)_3$, $Eu(OH)_3$ and LuO(OH)), aiming to the synthesis of phase-pure cubic $SmLuO_3$ and $EuLuO_3$ materials at high temperatures. The thermal behavior of nanostructured hydrothermally-derived precursors (samarium and europium hydroxides and lutetium oxy-hydroxides) was investigated in detail by X-ray diffraction, Raman spectroscopy, scanning and transmission electron microscopies. Our procedures allowed us to synthesize phase-pure cubic $SmLuO_3$ and $EuLuO_3$ materials belonging to the $Ia\bar{3}$ (#206) space-group. Crystal structures, morphological features and phonon modes were studied and assigned, thus contributing to the understanding of the role of the hydrothermal processing on the synthesis of these materials at high temperatures.

2. Experimental section

$SmLuO_3$ and $EuLuO_3$ were synthesized by using stoichiometric amounts of lanthanide nitrates, $Sm(NO_3)_3{\cdot}6H_2O$ and $Eu(NO_3)_3{\cdot}5H_2O$ (Sigma–Aldrich, purity >99.9%), and lutetium oxide (Lu_2O_3, Sigma–Aldrich, purity >99.9%) as starting materials. Because the lanthanide nitrates are highly hygroscopic, the amount of water was firstly checked prior to the experiments. Also, lutetium oxide was treated with HNO_3 65% to produce lutetium nitrate, according to the chemical reaction:

$$Lu_2O_3 + 6HNO_3 \rightarrow 2Lu(NO_3)_3 + 3H_2O \quad (1)$$

Lanthanide nitrate hydrate was introduced and mixed to the mother solution followed by addition of NaOH (10 mol/L) until the pH reach values above 13 under vigorous stirring. The resulting solutions were loaded into stainless steel Parr® autoclaves equipped with pressure and temperature controllers. The reaction vessels were heated at 10 °C/min up to the processing temperature and saturated vapor pressure (250 ± 1 °C and 580 ± 2 psi), for 24 h. After synthesis, the produced powders were washed with distilled water in order to remove any remaining Na^+ ion and dried. The general chemical reaction for the synthesis of the reactive precursors can be written as follows:

$$Lu(NO_3)_3 + Ln(NO_3)_3 + 6NaOH \rightarrow LuO(OH) + Ln(OH)_3 + 6NaNO_3 + H_2O. \quad (2)$$

The nanostructured precursors were calcined in conventional high-temperature muffle furnaces (air atmosphere) in the temperature range 800–1600 °C for fixed times of 10 h in order to investigate their thermal behavior and reactivity.

The crystal structure of the samples was studied by X-ray diffraction (XRD) using a Shimadzu D-6000 diffractometer with graphite monochromator and a nickel filter in the range of 10–60° 2θ (15 s/step of 0.02 °2θ), operating with Fe Kα radiation (λ = 0.1936 nm), 40 kV and 20 mA (the results were automatically converted to Cu Kα radiation for data treatment and manipulation). The software MDI Jade 9.0 was employed to calculate the lattice parameters. Micro-Raman spectra were collected in back-scattering configuration by using an Olympus confocal microscope (100× objective) attached to a Horiba/Jobin-Yvon LABRAM-HR spectrometer, and equipped with 600 and 1800 grooves/mm diffraction gratings. The 632.8 nm line of a He–Ne laser (maximum effective power of 6 mW at the surface of each sample) was used as exciting line and a Peltier-cooled charge coupled device (CCD) detected the scattered light. An edge filter was employed to stray light rejection (Rayleigh line). In order to avoid any kind of crystallization due to laser exposition, very low intensities were employed, beside lens with low magnification and defocused laser, when

Table 1 Phonon frequencies, FWHM and assignment of the *gerade* modes for the phase-pure cubic $SmLuO_3$ and $EuLuO_3$. The assignment was performed according to Schaac and Koningstein (1970), Repelin et al. (1995), Laversenne et al. (2001).

Bands #	Assignment	$SmLuO_3$		$EuLuO_3$	
		Frequency (cm^{-1})	FWHM (cm^{-1})	Frequency (cm^{-1})	FWHM (cm^{-1})
1	T_g	60.4	3	59.2	4
2	T_g	95.0	3	95.0	2
3,4	$T_g \oplus A_g$	118.3 + 119.2	2 + 3	117.9 + 118.8	2 + 3
5	T_g	134.5	2	134.7	3
6,7	$T_g \oplus E_g$	143.8 + 145.0	2 + 2	144.8 + 147.1	2 + 2
8	T_g	312.2	48	313.4	54
9,10	$T_g \oplus E_g$	334.9	22	335.5	24
11,12	$T_g \oplus A_g$	353.7 + 361.1	18 + 14	354.9 + 363.5	20 + 18
13	T_g	369.4	16	372.0	15
14,15	$T_g \oplus E_g$	421.2	13	422.6	10
16,17	$T_g \oplus A_g$	460.2 + 466.3	16 + 8	465.8 + 468.2	19 + 5
18	T_g	560.5	9	567.1	7
19,20	$T_g \oplus E_g$	564.3	7	568.2	5
21,22	$T_g \oplus A_g$	581.6	25	583.5	32

possible. Accumulation times of typically 20 collections of 10 s were employed with spectral resolution better than 1 cm^{-1}.

A Quanta FEG 3D (FEI) field-emission scanning electron microscope (FESEM) equipped with energy-dispersive spectrometer (EDS) was employed to analyze the morphology and chemical features of the $SmLuO_3$ and $EuLuO_3$-derived materials (applied voltages varied from 5 to 30 kV). Images were taken in both detection modes, i.e., secondary (SE) and backscattered (BSE) electrons, in order to differentiate the precursors and final compounds. High-resolution transmission electron microscopy (HRTEM) was carried out to investigate the crystalline aspects of the nanopowders in a Tecnai G2-20 (FEI) transmission microscope (applied voltage of 200 kV). We apply also nanobeam diffraction (NBD) mode in addition to HRTEM for acquiring diffraction patterns from selected areas of samples calcined at higher temperatures. A beam diameter of about 2 nm was used with the smallest condenser aperture. The resulting diffraction patterns were interpreted like a selected-area diffraction pattern.

3. Results and discussion

Fig. 1 presents XRD patterns and Raman spectra (Sm and Eu are displayed in black and red lines, respectively) obtained for the precursors hydrothermally synthesized at 250 °C. The XRD results (Fig. 1a) showed that $Sm(OH)_3$, $Eu(OH)_3$ and LuO(OH) were produced and could be indexed according to the ICDD (International Committee for Diffraction Data) cards #01-083-2036, #01-083-2305 and #01-072-0928, respectively. Fig. 1b presents the Raman spectra for the precursors hydrothermally synthesized at 250 °C. As it can be seen, a set of relatively broad Raman modes in the region 100–1050 cm^{-1} correspond to the $Sm(OH)_3$, $Eu(OH)_3$ and LuO(OH) vibrations. The bands related to LuO(OH) remain unchanged in both systems, such as below 200 cm^{-1} and those centered at 410, 660 and 830 cm^{-1}. For samarium and europium hydroxides, there are bands that do not change significantly their frequencies, like the modes at 302/305 and 380/382 cm^{-1} (Sm/Eu) (Kang et al., 2014; Swanson et al., 1978). On the other hand, the bands centered at around 480 and 595 cm^{-1} present very different intensities, being stronger in $Eu(OH)_3$ precursors in comparison with $Sm(OH)_3$ (Kang et al., 2014; Swanson et al., 1978).

Following, the thermal evolution aiming to the production of phase-pure cubic $SmLuO_3$ and $EuLuO_3$ materials from hydrothermal-derived precursors was studied in the temperature range 800–1600 °C. Fig. 2 shows the XRD results for the sample heat treated for 10 h at selected temperatures (800, 1000, 1200, 1400 and 1600 °C). Samples calcined at 800 °C have converted to lanthanide oxides and could be indexed according to the ICDD cards #01-076-0153 (Sm_2O_3), #01-073-6441 (Eu_2O_3) and #01-072-6366 (Lu_2O_3). Samarium and europium oxides belong to the $I2_13$ space group (#199), while lutetium oxide belongs to the $Ia\bar{3}$ (#206) space group (cubic fluorite-type phase). The lattice parameters were calculated for the two systems: a = 10.81 Å (Sm_2O_3) and a = 10.34 Å (Lu_2O_3), for the $SmLuO_3$ system, while a = 10.79 Å (Eu_2O_3) and a = 10.38 Å (Lu_2O_3), for the $EuLuO_3$ system. These lattice parameters changed for increasing temperatures, as expected, reaching values at 1200 °C of a = 10.80 Å (Sm_2O_3) and a = 10.37 Å (Lu_2O_3), for the $SmLuO_3$ system, and values of a = 10.81 Å (Eu_2O_3) and 10.35 Å (Lu_2O_3), for the $EuLuO_3$ system. The phase evolution with temperature reaches 1400 °C, now exhibiting mixed cubic $Ia\bar{3}$ space group and monoclinic $C2/m$ $SmLuO_3$ or $EuLuO_3$ materials (see Fig. 2b, which focuses on the range 25–35° 2Θ). At 1400 °C, the beginning of the chemical reactions between samarium or europium and lutetium oxides toward the formation of cubic solid solutions must be noted (Fig. 2b). For comparison, Fig. S1 (Supporting Information) presents XRD patterns for monoclinic Sm and Eu oxides along with our experimental data at 1400 °C. As it can be seen, these monoclinic polymorphs do not match with the secondary phase detected, which proves that monoclinic $SmLuO_3$ and $EuLuO_3$ materials are present at 1400 °C. Finally, at 1600 °C, solid solution could be formed between the lanthanide oxides and both $SmLuO_3$ and $EuLuO_3$ become visible as phase-pure, high crystallinity cubic materials, belonging to the $Ia\bar{3}$ space group (#206). The mean crystallite sizes were calculated by using the Scherrer's equation as 41 nm, for $EuLuO_3$, and 54 nm, for $SmLuO_3$.

According to the literature discussed above, perovskite-like $SmLuO_3$ and $EuLuO_3$ were not previously obtained

(Schneider and Roth, 1960; Su et al., 1988). In fact, the structural stability and formability of perovskite compounds are based on the so-called tolerance factor (t), a criterion proposed by Goldschmidt and discussed by Zhang et al., 2007. In an ideal cubic perovskite structure, the tolerance factor is equal to the unity. Lower t values may occur, which means that distorted structures are usually present. It has been accepted that almost all perovskites have t values ranging from 0.75 to 1.00. However, the tolerance factor is a necessary but not a sufficient condition for the formation of perovskite structures. The criterion proposed by Goldschmidt very often neglects the influence of the coordination number on the effective ionic radii, and was debated by the literature by years without a well defined criterion. For $SmLuO_3$ and $EuLuO_3$, the tolerance factors could be calculated as 0.7753 and 0.7712, respectively, which indicates that these compounds could be produced in distorted perovskite-like phases even if one considers these values near to the border for the traditional perovskite atomic arrangement. That is the case for some orthorhombic $LnLn'O_3$ (e.g. $LaLuO_3$, $LaYbO_3$, $PrLuO_3$) interlanthanides. In this work, the phase behavior followed by our $SmLuO_3$ and $EuLuO_3$ materials was quite different, since the hydrothermal precursors started forming cubic solid solutions between the lanthanide oxides at around 1400 °C. Beside, secondary monoclinic phase at this temperature was detected only as an impurity phase. Further increase in the temperature did destabilize the monoclinic phase, allowing the production of phase-pure cubic ($Ia\bar{3}$, #206) compounds at 1600 °C. Perovskite-like phases (orthorhombic) were not detected in our experiments for all conditions employed in this study. Fig. S2 (Supporting Information) presents XRD data for the phase-pure cubic $SmLuO_3$ and $EuLuO_3$ materials together with their Miller indexes (Alonso et al., 2004). The lattice parameters were determined for the cubic $Ia\bar{3}$ space group (Cullity, 1978) as a = 10.64 Å (V = 1204.8 Å^3), for $SmLuO_3$, and a = 10.61 Å (V = 1193.7 Å^3) for $EuLuO_3$.

The thermal behavior of hydrothermally treated precursors for the synthesis of $SmLuO_3$ and $EuLuO_3$ was also monitored by Raman scattering. Fig. 3 presents spectra for the samples sequentially treated at 800 °C, 1000 °C, 1200 °C, 1400 °C and 1600 °C. The spectra for the samples heat treated at 800 °C exhibit bands related to Lu_2O_3 (Ubaldini and Carnasciali, 2008), Sm_2O_3 (Martel et al., 1998) and Eu_2O_3 (Kang et al., 2014). The strongest bands for these compounds are located, respectively, at 390, 350 and 425 cm^{-1}. For the samples prepared at 1000 °C and 1200 °C, we can observe the same bands as for the sample produced at 800 °C, but with different relative intensities. At 1400 °C, monoclinic $SmLuO_3$ and $EuLuO_3$ can now be observed, in accordance with Mele et al. (2009), Tompsett et al. (1998) and Heiba et al. (2012), particularly in the frequency range 350–500 cm^{-1} for the same crystal structure ($C2/m$ space group). The Raman spectra for the samples produced at 1400 °C also present bands related to the cubic phase, for example at 370 cm^{-1}, for $SmLuO_3$, and 362 cm^{-1}, for $EuLuO_3$. The most characteristic bands for each of the observed phases are indicated by symbols in the figures.

The spectra for the samples calcined at 1600 °C (Fig. 3a and b, top) show the Raman-active modes for the phase-pure $SmLuO_3$ and $EuLuO_3$. For the corresponding cubic $Ia\bar{3}$ space group, there are sixteen formula units per unitary cell (Z = 16). The cations are distributed into two special Wyckoff positions: *8b* (C_{3i} local symmetry, for Sm or Eu) and *24d* (C_2 symmetry, for Lu), while the oxygen ions are located into *48e* general Wyckoff positions with C_1 symmetry (Marezio, 1966). Based on these occupation sites, the site-group method of Rousseau et al. (1981) was applied to obtain the following Raman-active modes:

$$\Gamma_{\mathrm{RAMAN}} = 4A_g \oplus 4E_g \oplus 14T_g \quad (3)$$

The results depicted in Fig. 3 show that all the 22 predicted bands are not easily visualized for either $SmLuO_3$ or $EuLuO_3$ treated at 1600 °C, which indicates that additional data procedures are necessary for analyzing the spectra. Therefore, the Raman spectra for these samples were fitted by Lorentzian curves and the results are presented in Fig. 4. The results showed that 18 Raman lines could be depicted (green curves) for both samples, in very good agreement with the theoretical predictions. Based on these fitted spectra, Table 1 presents the frequencies and full-width at half maxima (FWHM) for all observed bands and their proposed assignment (Schaac and Koningstein, 1970; Repelin et al., 1995; Laversenne et al., 2001; Jinqiu et al., 2014). In accordance with the previous literature, the Raman spectra depicted in Fig. 4 could represent a fingerprint of the cubic $Ia\bar{3}$ structure of $SmLuO_3$ and $EuLuO_3$ materials. We notice that accidental (or quasi-accidental) degeneracy between the orthogonal modes $T_g \oplus A_g$ (modes 21,22 in Table 1) or $T_g \oplus E_g$ (modes 9,10; 14,15; and 19,20 in Table 1) prevents the observation of all the 22 *gerade* modes for these materials, due to the polycrystalline nature of the samples. This only would be possible by using polarized light in appropriately oriented crystals or micro-crystals, which is not the present case. It is important to note the occurrence of very narrow Raman modes (see Table 1), which indicates that our samples exhibit high crystallinity (as also verified by XRD data) and superior long-range ordering degree. These characteristics could designate the phase-pure cubic materials obtained in the present work as promising candidates for advanced optical applications.

The thermal behavior of the resulting materials after heating was also investigated by FESEM and HRTEM. Typical samples, starting from the hydrothermally-treated precursors as well as the produced nanostructured interlanthanide oxides were examined in their morphological, chemical and structural aspects. Due to the similarity between the results for $SmLuO_3$ and $EuLuO_3$, the data for the $SmLuO_3$ materials were omitted. Fig. 5 presents a sequence of FESEM images (secondary electrons or SE, and backscattering electrons or BSE) for $EuLuO_3$ samples obtained under different processing conditions. First, Fig. 5a (SE) shows nanosized, agglomerated particles observed for the precursors synthesized by hydrothermal processing at 250 °C, for 24 h. As it can be seen, two different morphologies are present and could be associated after chemical EDS analyses with the precursors obtained after synthesis. LuO(OH) exhibits tabular, faceted particles (identified in Fig. 5a), while $Eu(OH)_3$ shows nanostructured, heavily agglomerated particles. Fig. 5b–e shows representative FESEM images (BSE) for our $EuLuO_3$ calcined in the temperature range 800–1600 °C. It was observed a generalized increase in their particle sizes; in particular, the morphologies due to LuO(OH) and $Eu(OH)_3$ changed above 800 °C (Fig. 5b and c) because of the conversion to the lanthanide oxides. EDS analyses showed that Lu and Eu are still in opposite corners, which means that a chemical reaction between these precursors was not in

progress. Fig. 5d and e presents the morphology of the samples obtained at 1400 °C and 1600 °C, which exhibit features of materials where some solid-state reaction could not be neglected. Hard, compacted agglomerates can be seen, which indicate that a chemical reaction between the hydrothermally-derived precursors has now occurred. In fact, EDS analyses indicate that it is not possible to discern between lutetium and europium along the materials anymore.

Fig. 6 shows representative HRTEM images obtained for $EuLuO_3$ samples produced at 1400 °C and 1600 °C. Also, electron nanobeam diffraction (NBD) was used to improve the characterization of the polycrystalline samples obtained at these higher temperatures (Cowley, 2004). Strong electromagnetic lenses were used to focus on intense electron beams (200 kV) to diameters of 1 nm or less. In this configuration, the scattered electrons are so strong that, when a bright source such as a field emission gun (FEG) is used, a diffraction pattern can be observed on a plane of observation distant from the sample and recorded using a CCD camera (Cowley, 2004). For our samples produced at 1400 °C, it was observed the presence of monoclinic $EuLuO_3$ phase, corroborating the results from XRD and Raman scattering. Fig. 6a presents a HRTEM image for this secondary phase, which exhibits interplanar spacing of about 2.86 Å corresponding to the (003) planes of the monoclinic $C2/m$ structure. The inset in Fig. 6a shows the respective NBD pattern, which agrees with a monoclinic space group. Fig. 6b presents a HRTEM image for the phase-pure cubic $EuLuO_3$ obtained at 1600 °C. Interplanar spacing was computed to be about 4.33 Å and 3.06 Å, which correspond to the (112) and (222) planes, respectively, for the cubic $Ia\bar{3}$ space group. The inset in Fig. 6b exhibits its NBD pattern, which evidenced the nice crystallinity of the phase-pure sample produced at 1600 °C. Also, the diffraction recorded from this area gives a very high resolution and is consistent with cubic close-packed stacking.

4. Conclusions

In this work, phase-pure cubic $SmLuO_3$ and $EuLuO_3$ interlanthanides were synthesized for the first time from nanostructured hydrothermally-derived precursors. Aqueous solutions of lutetium and samarium or europium nitrates were hydrothermally treated at 250 °C for 24 h in order to produce nanostructured LuO(OH), $Sm(OH)_3$ and $Eu(OH)_3$ precursors. The thermal behavior of the mixtures of these precursors was investigated by XRD, micro-Raman spectroscopy and electron microscopy (FESEM and HRTEM). It was observed that the precursors were converted to cubic lanthanide oxides at 800 °C, whose crystal structure did not change up to 1200 °C. Monoclinic and cubic $SmLuO_3$ and $EuLuO_3$ materials were observed for samples thermally treated at 1400 °C. Phase-pure cubic ($Ia\bar{3}$ space group, #206) materials were obtained only at 1600 °C, as verified by XRD, Raman spectroscopy and transmission electron microscopy. In order to check these findings, micro-Raman scattering was used to probe the phonon modes in cubic samples, which were determined and assigned. After fitting procedures, it was observed a total of 18 bands among the 22 modes predicted by group theory calculations for the $Ia\bar{3}$ structure, confirming the production of phase-pure cubic interlanthanides at 1600 °C.

Acknowledgments

The authors acknowledge the financial support from CAPES, CNPq, FINEP and FAPEMIG. The Center of Microscopy at the Universidade Federal de Minas Gerais (http://www.microscopia.ufmg.br) is also acknowledged for providing the equipment and technical support for experiments involving electron microscopy.

Appendix A. Supplementary material

Additional XRD data for samples produced at 1400 °C and 1600 °C. Supplementary data associated with this article can be found, in the online version, at http://dx.doi.org/10.1016/j.arabjc.2016.03.010.

References

Alonso, J.A., Casais, M.T., Martínez-Lope, M.J., 2004. Preparation and topotactical oxidation of $ScVO_3$ with bixbyte structure: a low-temperature route to stabilize the new defect fluorite $ScVO_{3.5}$ metastable phase. Dalton Trans. 9, 1294–1297.

Antic, B., Kremenovic, A., Vucinic-Vasic, M., Dohcevic-Mitrovic, Z., Nikolic, A.S., Gruden-Pavlovic, M., Lancar, B., Meden, A., 2010. Composition related properties of $(Yb,Y)_2O_3$ nanoparticles synthesized by controlled thermal degradation of AA complexes. Mater. Chem. Phys. 122, 386–391.

Artini, C., Costa, G.A., Masini, R., 2011. Study of the formation temperature of mixed $LaREO_3$ (RE = Dy, Ho, Er, Tm, Yb, Lu) and $NdGdO_3$ oxides. J. Therm. Anal. Calorim. 103, 17–21.

Azimi, G., Dhiman, R., Kwon, H., Paxson, A., Varanasi, K., 2013. Hydrophobicity of rare-earth oxide ceramics. Nat. Mater. 12, 315–320.

Bharathy, M., Fox, A.H., Mugavero, S.J., zur Loye, H.-C., 2009. Crystal growth of inter-lanthanide $LaLn'O_3$ (Ln′ = Y, Ho–Lu) perovskites from hydroxide fluxes. Solid State Sci. 11, 651–654.

Blanusa, J., Jovic, N., Dzomic, T., Antic, B., Kremenovic, A., Mitric, M., Spasojevic, V., 2008. Magnetic susceptibility and ordering of Yb and Er in phosphors Yb, Er:Lu_2O_3. Opt. Mater. 30, 1153–1156.

Byrappa, K., Yoshimura, M., 2001. Handbook of Hydrothermal Technology. William Andrew Publishing, New York.

Chung, D.Y., Lee, E.H., 2004. Microwave-induced combustion synthesis of $Ce_{1-x}Sm_xO_{2-x/2}$ powder and its characterization. J. Alloys Compd. 374, 69–73.

Cowley, J.M., 2004. Applications of electron nanodiffraction. Micron 35, 345–360.

Cullity, B.D., 1978. Elements of X-ray Diffraction, second ed. Addison-Wesley Publishing Company Inc, Massachusetts.

Dakhel, A.A., 2004a. Dielectric and optical properties of samarium oxide thin films. J. Alloys Compd. 365, 233–239.

Dakhel, A.A., 2004b. Characteristics of deposited Eu_2O_3 film as a thick gate dielectric for silicon. Eur. Phys. J. Appl. Phys. 28, 59–64.

Dias, A., Ciminelli, V.S.T., 2003. Electroceramic materials of tailored phase and morphology by hydrothermal technology. Chem. Mater. 15, 1344.

Dias, A., Moreira, R.L., 2007. Production of Sr-deficient bismuth tantalates from microwave-hydrothermal derived precursors: structural and dielectric properties. J. Phys. Chem. Solids 68, 645–649.

Dias, A., Ciminelli, V.S.T., Matinaga, F.M., Moreira, R.L., 2001. Raman scattering and X-ray diffraction investigations on hydrothermal barium magnesium niobate ceramics. J. Eur. Ceram. Soc. 21, 2738–2744.

Dias, A., Matinaga, F.M., Moreira, R.L., 2007. Raman spectroscopy of $(Ba_{1-x}Sr_x)(Mg_{1/3}Nb_{2/3})O_3$ solid solutions from microwave-hydrothermal powders. Chem. Mater. 19, 2335–2341.

Dias, A., Matinaga, F.M., Moreira, R.L., 2009. Vibrational spectroscopy and electron-phonon interactions in microwave-hydrothermal synthesized $Ba(Mn_{1/3}Nb_{2/3})O_3$ complex perovskites. J. Phys. Chem. B 113, 9749–9755.

Dubok, V.A., Lashneva, V.V., Kryuchkov, Y.N., 2003. Electrophysical properties of oxide interlanthanides and solid solutions based on them. Glass Ceram. 60, 115–117.

Gao, J., Zhao, Y., Yang, W., Tian, J., Guan, F., Ma, Y., Hou, J., Kang, J., Wang, Y., 2002. Preparation of samarium oxide nanoparticles and its catalytic activity on the esterification. Mater. Chem. Phys. 77, 65–69.

Hao, J., Li, Y.W., Wang, J.S., Ma, C.L., Huang, L.Y., Liu, R., Cui, Q. L., Zou, G.T., Liu, J., Li, X.D., 2010. Experimental determinations of the high-pressure crystal structures of Ca_3N_2. J. Phys. Chem. C 114, 16750–16755.

Heiba, Z.K., Akin, Y., Sigmund, W., Hascicek, Y.S., 2003. X-ray structure and microstructure determination of the mixed sesquioxides $(Eu_{1-x}Yb_x)_2O_3$ prepared by a sol–gel process. J. Appl. Cryst. 36, 1411–1416.

Heiba, Z.K., Arda, L., Hascicek, Y.S., 2005. Structure and microstructure characterization of the mixed sesquioxides $(Gd_{1-x}Yb_x)_2O_3$ and $(Gd_{1-x}Ho_x)_2O_3$ prepared by sol–gel process. J. Appl. Cryst. 38, 306–310.

Heiba, Z.K., Mohamed, M.B., Fuess, H., 2012. XRD, IR, and Raman investigations of structural properties of $Dy_{2-x}Ho_xO_3$ prepared by sol gel procedure. Cryst. Res. Technol. 47, 535–540.

Ito, K., Tezuka, K., Hinatsu, Y., 2001. Preparation, magnetic susceptibility, and specific heat on interlanthanide perovskites ABO_3 (A = La–Nd, B = Dy–Lu). J. Solid State Chem. 157, 173–179.

Jinqiu, Y., Lei, C., Huaqiang, H., Shihong, Y., Yunsheng, H., Hao, W., 2014. Raman spectra of RE_2O_3 (RE = Eu, Gd, Dy, Ho, Er, Tm, Yb, Lu, Sc and Y): laser-excited luminescence and trace impurity analysis. J. Rare Earths 32, 1–4.

Kang, J.-G., Jung, Y., Min, B.-K., Sohn, Y., 2014. Full characterization of $Eu(OH)_3$ and Eu_2O_3 nanorods. Appl. Surf. Sci. 314, 158–165.

Laversenne, L., Guyot, Y., Goutaudier, C., Cohen-Adad, M.Th, Boulon, 2001. Optimization of spectroscopic properties of Yb^{3+}-doped refractory sesquioxides: cubic Y_2O_3, Lu_2O_3 and monoclinic Gd_2O_3. Opt. Mater. 16, 475–483.

Marezio, M., 1966. Refinement of the crystal structure of In_2O_3 at two wavelengths. Acta Cryst. 20, 723.

Martel, J.-F., Jandl, S., Lejus, A.M., Viana, B., Vivien, D., 1998. Optical crystal field study of Sm_2O_3 (C- and B-type). J. Alloys Compd. 275–277, 353–355.

Mele, P., Artini, C., Masini, R., Costa, G.A., Hu, A., Chikumoto, N., Murakami, M., 2003. Synthesis and superconductive characterisation of $RuSr_2Nd_xGd_{1-x}Cu_2O_8$ compounds (x = 0, 0.09, 0.18, 0.35). Physica C 391, 49–54.

Mele, P., Artini, C., Ubaldini, A., Costa, G.A., Carnasciali, M.M., Masini, R., 2009. Synthesis, structure and magnetic properties in the Nd_2O_3–Gd_2O_3 mixed system synthesized at 1200 °C. J. Phys. Chem. Solids 70, 276–280.

Moreira, R.L., Feteira, A., Dias, A., 2005. Raman and infrared spectroscopic investigation on the crystal structure and phonon modes of $LaYbO_3$ ceramics. J. Phys.: Condens. Matter 17, 2775–2781.

Panitz, J.C., Mayor, J.C., Grob, B., Durish, W., 2000. A Raman spectroscopic study of rare earth mixed oxides. J. Alloys Compd. 303–304, 340–344.

Paranthaman, M., Lee, D.F., Goyal, A., Specht, E.D., Martin, P.M., Cui, X., Mathis, J.E., Feenstra, R., Christen, D.K., Kroeger, D.M., 1999. Growth of biaxially textured RE_2O_3 buffer layers on rolled-Ni substrates using reactive evaporation for HTS-coated conductors. Supercond. Sci. Technol. 12, 319–325.

Peng, C., Zhang, Z., 2007. Nitrate–citrate combustion synthesis of $Ce_{1-x}Gd_xO_{2-x/2}$ powder and its characterization. Ceram. Int. 33, 1133–1136.

Repelin, Y., Proust, C., Husson, E., Beny, J.M., 1995. Vibrational spectroscopy of the C-form of yttrium sesquioxide. J. Solid State Chem. 118, 163–169.

Rousseau, D.L., Bauman, R.P., Porto, S.P.S., 1981. Normal mode determination in crystals. J. Raman Spectrosc. 10, 253–290.

Schaac, G., Koningstein, J.A., 1970. Phonon and electronic Raman spectra of cubic rare-earth oxides and isomorphous yttrium oxide. J. Opt. Soc. Am. 60, 1110–1115.

Schneider, S.J., Roth, R.S., 1960. Phase equilibria in systems involving the rare-earth oxides. Part II. Solid state reactions in trivalent rare-earth oxide systems. J. Res. NBS 64A, 317–332.

Sharma, Y., Sahoo, S., Mishra, A.K., Misra, P., Pavunny, S.P., Dwivedi, A., Sharma, S.M., Katiyar, R.S., 2015. Structural phase transition of ternary dielectric $SmGdO_3$: evidence from angle-dispersive X-ray diffraction and Raman spectroscopic studies. J. Appl. Phys. 117, 094101.

Shionoya, S., Yen, W.M., 1999. Phosphor Handbook. CRC Press, Boca Raton.

Singh, M.P., Shalini, K., Shivashankar, S.A., Deepak, G.C., Bhat, N., Shripathi, T., 2008. Microstructure, crystallinity, and properties of low-pressure MOCVD-grown europium oxide films. Mater. Chem. Phys. 110, 337–343.

Siqueira, K.P.F., Dias, A., 2011. Incipient crystallization of transition-metal tungstates under microwaves probed by Raman scattering and transmission electron microscopy. J. Nanopart. Res. 13, 5927–5933.

Siqueira, K.P.F., Moreira, R.L., Valadares, M., Dias, A., 2010. Microwave-hydrothermal preparation of alkaline-earth-metal tungstates. J. Mater. Sci. 45, 6083–6093.

Su, Wenhui, Liu, Xiaoxiang, Jin, Mingzhi, Xu, Weiming, Wu, Daiming, Liu, Milan, 1988. Mossbauer effect used to study rare-earth oxides synthesized by a high-pressure method. Phys. Rev. B 37, 35–37.

Su, Wenhui, Xu, Weiming, Zhao, Xin, Liu, Xiaoxiang, Wu, Daiming, Jin, Mingzhi, 1989. ^{151}Eu Mossbauer effect in light rare-earth oxides. Phys. Rev. B 40, 102–105.

Swanson, B.I., Machell, C., Beall, G.W., Milligan, W.O., 1978. Vibrational spectra and assignments for the lanthanide trihydroxides. J. Inorg. Nucl. Chem. 40, 694–696.

Tamburini, S., Sitran, S., Peruzzo, V., Vigato, P.A., 2009. The role of functionalisation, asymmetry and shape of a new macrocyclic compartmental ligand in the formation of mononuclear, homo- and heterodinuclear lanthanide(III) complexes. Eur. J. Inorg. Chem., 155–167

Tompsett, G.A., Philips, R.J., Sammes, N.M., Cartner, A.M., 1998. Characterisation of $LaGdO_3$ by X-ray powder diffraction and Raman spectroscopy. Solid State Commun. 108, 655–660.

Tsuzuki, T., Harrison, W.T.A., McCormick, P.G.J., 1998. Synthesis of ultrafine gadolinium oxide powder by mechanochemical processing. J. Alloys Compd. 281, 146–151.

Ubaldini, A., Carnasciali, M.M., 2008. Raman characterization of powder of cubic RE_2O_3 (RE = Nd, Gd, Dy, Tm, and Lu), Sc_2O_3 and Y_2O_3. J. Alloys Compd. 454, 374–378.

Wang, J., Liu, T., Wang, Z., Bugiel, E., Laha, A., Watahiki, T., Shayduk, R., Braun, W., Fissel, A., Osten, H.J., 2010. Epitaxial multi-component rare-earth oxide: a high-k material with ultralow mismatch to Si. Mater. Lett. 64, 866–868.

Yang, H., Wang, H., Luo, H.M., Feldman, D.M., Dowden, P.C., Depaula, R.F., Jia, Q.X., 2008. Structural and dielectric properties of epitaxial Sm_2O_3 thin films. Appl. Phys. Lett. 92, 062905.

Yoshimura, M., Byrappa, K., 2008. Hydrothermal processing of materials: past, present and future. J. Mater. Sci. 43, 2085–2103.

Zhang, L., Zhu, H., 2009. Dielectric, magnetic, and microwave absorbing properties of multi-walled carbon nanotubes filled with Sm_2O_3 nanoparticles. Mater. Lett. 63, 272–274.

Zhang, H., Li, N., Li, K., Xue, D., 2007. Structural stability and formability of ABO_3-type perovskite compounds. Acta Cryst. B 63, 812–818.